








RESEARCH ARTICLE | JULY 13 2023

Freestanding graphene heat engine analyzed using stochastic thermodynamics

J. Durbin  ; J. M. Mangum  ; M. N. Gikunda; F. Harerimana; T. Amin  ; P. Kumar  ; L. L. Bonilla  ; P. M. Thibado  



AIP Advances 13, 075217 (2023)
<https://doi.org/10.1063/5.0147464>

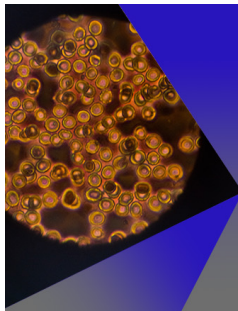


View Online



Export Citation

CrossMark



AIP Advances

Special Topic: Medical Applications of Nanoscience and Nanotechnology

Submit Today!

Freestanding graphene heat engine analyzed using stochastic thermodynamics

Cite as: AIP Advances 13, 075217 (2023); doi: 10.1063/5.0147464

Submitted: 22 February 2023 • Accepted: 24 June 2023 •

Published Online: 13 July 2023



View Online



Export Citation



CrossMark

J. Durbin,¹  J. M. Mangum,¹  M. N. Gikunda,¹ F. Harerimana,¹ T. Amin,¹  P. Kumar,¹  L. L. Bonilla,² 
and P. M. Thibado^{1,a)} 

AFFILIATIONS

¹Department of Physics, University of Arkansas, Fayetteville, Arkansas 72701, USA

²G. Millán Institute for Fluid Dynamics, Nanoscience and Industrial Mathematics and Department of Mathematics, Universidad Carlos III de Madrid, 28911 Leganés, Spain

^{a)}Author to whom correspondence should be addressed: thibado@uark.edu

ABSTRACT

We present an Ito-Langevin model for freestanding graphene connected to an electrical circuit. The graphene is treated as a Brownian particle in a double-well potential and is adjacent to a fixed electrode to form a variable capacitor. The capacitor is connected in series with a battery and a load resistor. The capacitor and resistor are given separate thermal reservoirs. We have solved the coupled Ito-Langevin equations for a broad range of temperature differences between the two reservoirs. Using ensemble averages, we report the rate of change in energy, heat, and work using stochastic thermodynamics. When the resistor is held at higher temperatures, the efficiency of the heat engine rises linearly with temperature. However, when the graphene is held at higher temperatures, the efficiency instantly rises and then plateaus. Also, twice as much entropy is produced when the resistor is hotter compared to when the graphene is hotter. Unexpectedly, the temperature of the capacitor is found to alter the dissipated power of the resistor.

© 2023 Author(s). All article content, except where otherwise noted, is licensed under a Creative Commons Attribution (CC BY) license (<http://creativecommons.org/licenses/by/4.0/>). <https://doi.org/10.1063/5.0147464>

I. INTRODUCTION

Modern circuit technology is capable of building circuits that consume picowatts of power in standby mode.¹ This ultralow power level presents an opportunity to consider using waste heat from the ambient environment as a battery alternative.

Newly discovered materials have demonstrated the possibility of harvesting ambient energy; for example, chemically doped single-wall carbon nanotubes (SWNTs) have been shown to be thermoelectric and capable of harvesting energy from low temperature (<400 K) heat dumps.² Thin layers of double-walled carbon nanotubes have yielded the highest thermoelectric figure of merit and may be able to harvest energy from body heat.³ Polyvinylidene fluoride was recently found to be pyroelectric and, thus, shows promise for energy harvesting from local temperature fluctuations.⁴ A composite made with ferricyanide was shown to generate thermoelectric power on the order of milliwatts per square meter.⁵ Two-dimensional materials, like doped molybdenum disulfide, have also demonstrated waste

heat energy harvesting.^{6,7} Silicene, or monolayer silicon, has been found to have an enhanced thermoelectric efficiency.⁸

Unusual mechanical properties of new systems also show promise for future heat engines; for example, bimetallic strips can undergo snap-through buckling and have demonstrated the potential as a heat engine.^{9,10} Particles in a laser trap undergo Brownian motion and can serve as a hot reservoir in a Stirling engine.^{11,12} Using an ion trap, it was shown that squeezed state can be used to generate power with an efficiency higher than the Carnot limit.¹³

Graphene is a durable, conductive two-dimensional material that has been proposed for use in harvesting energy from waste heat.¹⁴ Graphene was found to be a better thermal rectifier than carbon nanotubes.^{15–17} Graphene oxide membranes have been incorporated into osmotic heat engines.¹⁸ The high thermal conductivity of graphene 10^{10} W/(Km) has proven useful for dissipating heat in electronic devices.^{19,20} Additionally, the efficiency of thermophotovoltaic cells, which harvest energy from IR radiation, is predicted to be improved with the incorporation of graphene.²¹

One motivation for our project originates from a General Electric company study completed by Philp in 1977.²² Philp proposes a varying-capacitance machine and predicts the peak power to be $P_{\max} = f \Delta C V^2$, where f is the frequency, ΔC is the change in capacitance, and V is the bias voltage. To test this, our group built a varying-capacitance machine and demonstrated energy harvesting with an efficiency of 50% even when operated at one Hertz.²³ This machine generates a small amount of power but has the potential to replace batteries in low-power sensor applications.¹ Powering the Internet of Things is driving extensive research in this area.^{24–26} Graphene is thin, strong, and the most flexible material as flexural rigidity decreases with thickness to the third power. Graphene also has a high natural frequency (70 MHz), which helps offset the small capacitance occurring with small-size devices.²⁷ As a result, our group also built an array of nearly 100 000 graphene variable capacitors on a 100 mm silicon wafer using conventional semiconductor processing technology.²⁸ Each graphene variable capacitor consists of a well that was etched into the silicon surface. At the bottom, the center of the well is a fixed cone-shaped metal probe. Graphene is suspended over the well to form the variable capacitor. The tip of the metal probe is sized to be on the order of the size of an individual graphene ripple. We confirmed, using capacitance and resistance measurements, that the graphene membrane is freestanding, always moving, and provides a varying capacitance necessary for energy harvesting.

The dynamics of an individual ripple have been extensively studied using state-of-the-art molecular dynamics simulations.²⁹ The ripple inverts its curvature similar to a snap-through phenomenon. Convex and concave ripples represent the two lowest-energy configurations. The curvature inversion is quick and infrequent. The dynamics of the ripple were shown previously to be accurately modeled as a Brownian particle in a double-well potential.^{30,31} A key parameter in determining the barrier crossing rate is the lattice strain.

In this study, we take advantage of the naturally forming ripples of freestanding graphene, which can spontaneously invert its curvature between concave and convex states.^{32–36} When placed near a fixed electrode, a variable capacitor is formed and incorporated into an electrical circuit.

II. GRAPHENE AND CIRCUIT MODEL

A diagram for the model used is shown in Fig. 1(a). Starting with the fixed electrode and then moving clockwise, there is a load resistor, a battery, and a graphene ripple. The movement of the graphene ripple alters the capacitance of the circuit. A diagram labeling the sources of heat flux (two left components) and power (two right components) is shown in Fig. 1(b). Left to right, there is the graphene thermal bath at temperature T_G , the graphene ripple, the load resistor, and the resistor thermal bath at temperature T_R .

The graphene membrane is a single compressed ripple, which can have either a concave or a convex curvature.³⁷ The ripple is then modeled as a single Brownian particle subject to a double well potential, which is in contact with a thermal bath at temperature T_G . The Ito-Langevin equations for the graphene, which were presented in an earlier study,³¹ are as follows:

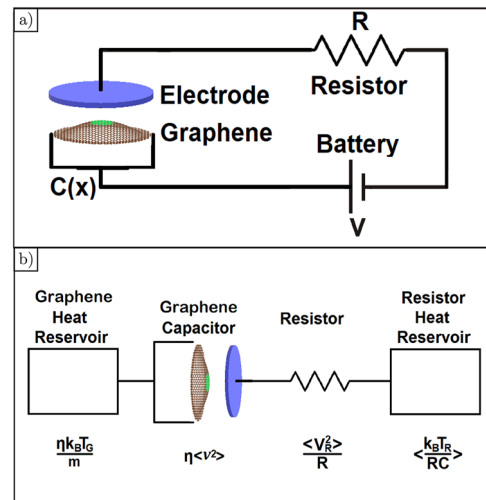


FIG. 1. (a) Circuit diagram showing our model. (b) Illustration showing the two heat baths, graphene friction, and resistor dissipation.

$$\dot{x} = v, \tag{1a}$$

$$m\dot{v} = -\eta v - U'(x) - \frac{q^2 - C_0^2 V^2}{2C_0 d} + \sqrt{2k_B T_G \eta} \xi_v(t), \tag{1b}$$

$$C(x) = \frac{C_0}{\left(1 + \frac{x}{d}\right)}, \tag{1c}$$

$$U(x) = x^4 - 2x^2, \tag{1d}$$

where $-\eta v$ is the damping force and $-\frac{q^2 - C_0^2 V^2}{2C_0 d}$ is the electrostatic force on the graphene with a correction for tension due to graphene's ability to stretch, $\sqrt{2k_B T_G \eta} \xi_v(t)$ is the thermal force, ξ_v is a zero-mean delta-correlated white noise, $C(x)$ is the graphene capacitance, $C_0 = \frac{\epsilon_0 A}{d}$, A is the area of the graphene, and $U(x)$ is the double well potential.

The damping force or friction term allows the transfer of kinetic energy from the ripple to the graphene lattice. The strength of the thermal noise enables the fluctuation–dissipation theorem to hold, thereby producing an overall thermal equilibrium if the graphene and circuit are at the same temperature.

The electrostatic energy is proportional to the square of the capacitor charge divided by its capacitance. As the latter is inversely proportional to the position of the graphene ripple, the energy is linear with the ripple position, which produces a constant electrostatic force. Equation (1b) also includes a correction for tension due to the graphene's ability to stretch.³¹

As the graphene fluctuates between the two equilibrium positions, the distance $d + x(t)$ is the instantaneous separation between the plates, and $x(t)$ is the displacement from the average (located midway between the two equilibrium positions).

Applying Kirchhoff's loop rule to the circuit schematic and adding the stochastic noise term yields the following circuit equation:

$$\dot{q} = -\frac{1}{R} \left(\frac{q}{C(x)} + V \right) + \sqrt{\frac{2k_B T_R}{R}} \xi_q(t), \quad (2)$$

where $\sqrt{\frac{2k_B T_R}{R}} \xi_q(t)$ is the stochastic current, and ξ_q is another zero-mean independent white noise. The resistor is in contact with its thermal bath, which is held at temperature T_R .

We perform numerical simulations of the stochastic model Eqs. (1) and (3) using the Euler–Maruyama method. We have chosen parameters that allow the simulation to capture the important physics in a qualitative manner. We have used the following parameters in all the numerical simulations $m = 1$, $V = 1$, $C_0 = 1$, and $d = 5$. Also, the double-well potential has a minimum of ± 1 and an energy barrier of 1. Other adjusted parameters are presented later. To ensure numerical convergence, simulations used a time step of 0.000 05, 10×10^6 timesteps, and 100 realizations.

To quantify and track the non-equilibrium rates of change in energy, heat, and work, we use stochastic thermodynamics.^{38–43} From the point of view of the graphene ripple, represented by Eq. (1), the circuit is an external system that does work on it. We track the energy of the system using the following Hamiltonian:

$$\mathcal{H}(x, v, q) = \frac{mv^2}{2} + U(x) + \frac{q^2}{2C(x)} - \frac{C_0 V^2 x}{2d} + qV. \quad (3)$$

The energy consists of the kinetic energy of the graphene, the potential energy of the graphene, the energy stored on the capacitor, the elastic energy of the stretched graphene, and the energy of the battery, respectively. To track the heat flux, we use the following expression for our earlier study:³²

$$\left\langle \frac{dQ}{dt} \right\rangle = \frac{\eta}{m} (k_B T_G - m \langle v^2 \rangle). \quad (4)$$

The first term is the heat flux produced by the graphene thermal bath, and the second term is the heat flux dissipated by friction due to the movement of the graphene ripple. To track the power, we use the following expression:³²

$$\left\langle \frac{dW}{dt} \right\rangle = \left\langle \frac{k_B T_R}{RC(x)} \right\rangle - \left\langle \frac{V_R^2}{R} \right\rangle. \quad (5)$$

The first term is the power produced by the resistor thermal bath, and the second term is the power dissipated by the resistor.

III. POSITION AND CHARGE DYNAMICS WHILE INCREASING T_G

In this section, we present results when the temperature of the graphene bath T_G is varied, and the temperature of the resistor bath is kept fixed. We vary $k_B T_G$ to be 0.5, 5, 10, 20, 30, 40, and 50 and leave $k_B T_R$ fixed at 0.5. The other parameters are $R = 0.25$ and $\eta = 0.05$.

The simulation results for position and charge dynamics are shown in Fig. 2. When $k_B T_G = k_B T_R = 0.5$, the position of the graphene is shown in Fig. 2(a), and the charge on the graphene is shown in Fig. 2(b). The graphene’s position randomly moves between the two minima of the double well potential, while the average charge is -1 . The charge is expected to be -1 because $V = 1$ and $C_0 = 1$. When $k_B T_G$ is increased to 5, the position is shown

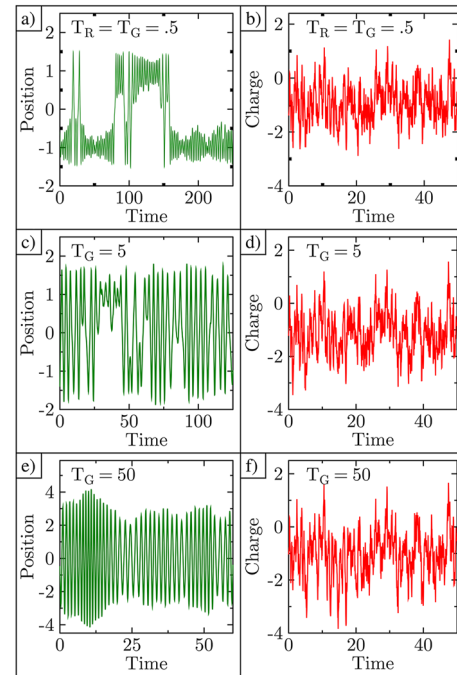


FIG. 2. Plots showing position and charge for various combinations of temperatures, where T_G is being varied and $k_B T_R = 0.5$. (a)–(b) $k_B T_G = 0.5$. (c)–(d) $k_B T_G = 5.0$. (e)–(f) $k_B T_G = 50$.

in Fig. 2(c), and the charge is shown in Fig. 2(d). Notice that the graphene is now rarely trapped on one side of the double well potential. The changes to the charge are subtler, but close inspection reveals that the charge has larger extremes; please see Fig. 3(d) for a plot of charge variance vs graphene temperature. Since the thermal bath of the graphene is hotter, the kinetic energy of the graphene is higher, and it crosses the barrier more often. The larger excursions result in larger capacitance variations and thus larger charge variations. For $k_B T_G = 50$, the position is shown in Fig. 2(e), and the charge is shown in Fig. 2(f). Here, the graphene oscillates back and forth in the double well potential as if it was in a single larger potential well. The graphene is never trapped on one side. Notice that the charge again reaches higher values throughout the simulation.

IV. RATES OF HEAT, WORK, AND ENERGY WHILE INCREASING T_G

From the dynamical data, we tracked energy rate, heat flux, and power as shown in Fig. 3. As the temperature of the graphene increases, the rate of change in energy is zero in time as expected and shown with red circles in Fig. 3(a). The heat flux starts off at zero when the temperatures are equal, this tells us the system has reached thermodynamic equilibrium. As the graphene temperature is increased above that of the resistor, we see a steady increase in the heat flux. Therefore, the thermal bath produces more heat than the frictional forces of the graphene can dissipate. As a result, the heat flux is positive.

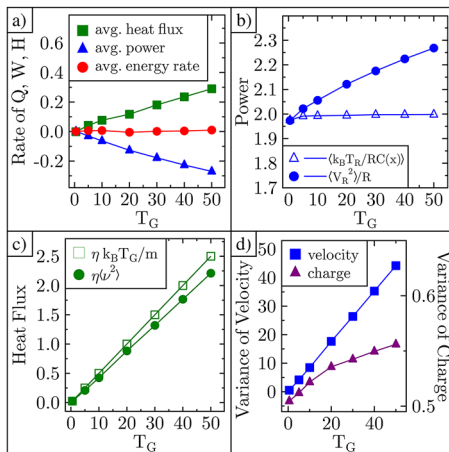


FIG. 3. Numerical simulations while varying T_G . (a) Ensemble average heat flux, power, and energy rate. (b) Two power terms separately presented. (c) Two heat flux terms separately presented. (d) Variance of velocity and charge.

The temperature of the graphene is elevated but held constant in this simulation. The kinetic energy of the graphene ripple increases due to the heat flux. This added kinetic energy is the source of energy for the additional work done by the graphene on the circuit.

The power also starts off at zero because the system is in thermodynamic equilibrium. However, after that, the power becomes negative and steadily decreases. Negative power means that the resistor is dissipating more power than is being delivered by the thermal bath of the resistor. Therefore, the temperature of the capacitor does play a role in the power dissipated by the resistor. This is different than Nyquist’s prediction.⁴⁴

Notice that the heat flux and power are equal in magnitude and add to zero. This agrees with the first law of thermodynamics. What we can conclude is that the extra heat flux produced by the thermal bath of the graphene capacitor is dissipated by the load resistor.

From the dynamical simulation data, we separate the two power terms given in Eq. (5) and plot each in Fig. 3(b). The power produced by the thermal bath of the resistor is shown as open triangles, while the power dissipated by the resistor is shown as solid circles. Notice, except at the very lowest temperatures, that the power produced by the resistor thermal bath does not change as the temperature of the graphene thermal bath increases. This is because the power depends primarily on the temperature of the resistor’s thermal bath, but it does have a small dependence on the capacitance variations.

The dissipated power of the resistor increases as the temperature of the graphene thermal bath increases. Clearly, the temperature of the capacitor affects the power dissipated by the resistor.

The heat flux was also separated into the two terms given by Eq. (4), and we plot each in Fig. 3(c). The heat flux produced by the thermal bath of the graphene is shown as open squares and increases linearly with temperature as expected. The graphene friction heat flux term also increases as the thermal bath of the graphene temperature increases but at a slightly reduced rate.

We calculated the variance of the velocity of the graphene ripple and the variance of the charge in the circuit as shown

in Fig. 3(d). Both increase as the temperature of the graphene increases. The increase in the variance of the charge is much easier to see in this plot as compared to the charge–time plots presented earlier.

V. POSITION AND CHARGE DYNAMICS INCREASING T_R

In this section, we present results when the temperature of the resistor bath T_R is varied, and the temperature of the graphene bath is kept fixed. We vary $k_B T_R$ to be 0.5, 5, 10, 20, 30, 40, and 50 and leave $k_B T_G$ fixed at 0.5. The other changed parameters are $R = 10$ and $\eta = 1$. Note that R and η differ from the earlier simulations due to differing simulation convergence requirements.

To learn about the role of T_R in the dynamics, we plot the position and charge in Fig. 4. When the two temperatures are equal, the graphene spends an equal amount of time on each side of the double-well potential, as shown in Fig. 4(a). The charge dynamics was increased by a factor of 40. Nevertheless, the average charge is still -1 . When $k_B T_R = 5$, the graphene exhibits similar dynamics to the $k_B T_R = 0.5$ case but does spend more time closer to the electrode as shown in Fig. 4(c). The charge dynamics, on the other hand, have changed significantly. The extreme values for the charge are now closer to four instead of one. The average charge is still -1 , however. When $k_B T_R = 50$, the graphene now spends most of its time closest to the electrode, as shown in Fig. 4(e). Crossing events are quickly reversed, and the graphene experiences greater displacement in the negative direction

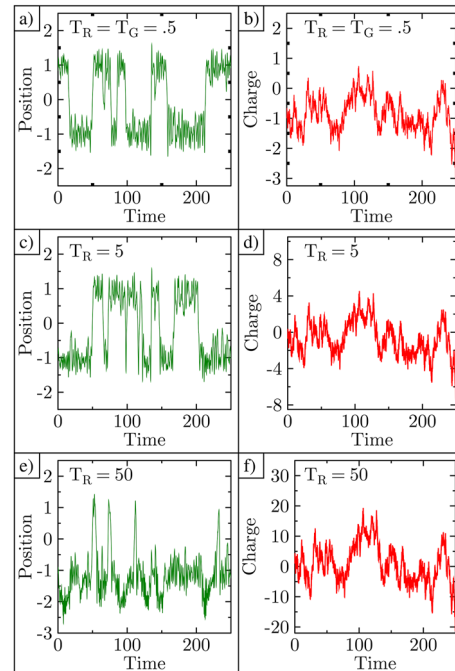


FIG. 4. Plots showing position and charge for various combinations of temperatures, where T_R is being varied and $k_B T_G = 0.5$. (a)–(b) $k_B T_R = 0.5$. (c)–(d) $k_B T_R = 5.0$. (e)–(f) $k_B T_R = 50$.

than in Fig. 4(c). The origin of this is clear when we review the charge dynamics shown in Fig. 4(f). Now the charge reaches a maximum of 20. We know the electrostatic force is always attractive and independent of the sign of the charge, so the graphene is pulled closer to the electrode when the charge deviates far from zero. The average charge is still maintaining a value of -1 .

Notice that the charge dynamics in the righthand column of Fig. 4 are nearly identical even though the scales are dramatically different. Here, we specifically chose to plot the simulation results for realizations using the same random number generator seed to highlight its lack of influence in setting the scale of the charges. Equation (2) indicates that the charge tries to relax to the average value -1 if the fluctuations in the position are symmetric [because $|x| < d$ and $C(x) = (1 + x/d)/C_0$ fluctuates near 1] or to a somewhat lower value otherwise, as in Fig. 4(e). The same equation shows that the scale of the charge fluctuation increases with the temperature T_R but the charge dynamics are similar.

VI. RATES OF HEAT, WORK, AND ENERGY WHILE INCREASING T_R

From the dynamical data, we tracked energy rate, heat flux, and power as shown in Fig. 5. As the temperature of the resistor increases, the rate of change in energy is zero in time as expected and shown with red circles in Fig. 5(a). However, unlike the earlier case, the sign of the power and heat flux are now opposite of what they were in Fig. 3(a). The heat flux starts at zero and becomes negative and decreases as the temperature of the resistor thermal bath increases. This tells us the graphene friction heat flux is now larger than the heat flux of the graphene thermal bath.

The power starts at zero, then becomes positive, and increases. This means the resistor thermal bath power is larger than the dissipated power of the resistor. As before and consistent with the first law, the power and heat flux terms add to zero.

Both power terms are separately found to increase with T_R as shown in Fig. 5(b). The power of the resistor thermal bath increases

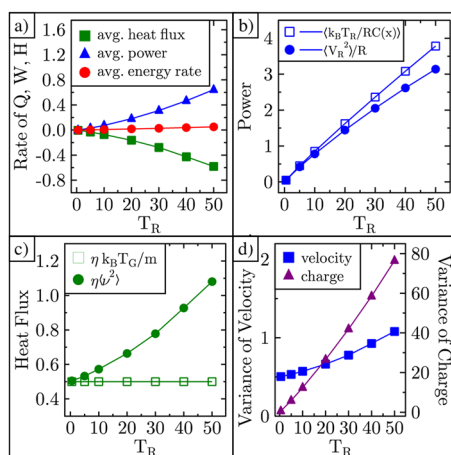


FIG. 5. Numerical simulations while varying T_R . (a) Ensemble average heat flux, power, and energy rate. (b) Two power terms separately presented. (c) Two heat flux terms separately presented. (d) Variance of velocity and charge.

linearly as expected. The dissipated power of the resistor increases as well but at a slower rate.

The heat flux of the graphene thermal bath is constant as expected and shown in Fig. 5(c). The heat flux due to friction does increase as the resistor's temperature increases.

The variance of velocity and charge both increase with temperature, as shown in Fig. 5(d).

VII. ENTROPY AND EFFICIENCY

A general expression for entropy production for our system is as follows:

$$\Sigma = \frac{1}{T_G} \left\langle \frac{d'Q}{dt} \right\rangle - \frac{1}{T_R} \left\langle \frac{d'W}{dt} \right\rangle. \quad (6)$$

Using the first law and that the rate of change in energy is zero, Eq. (6) can be expressed in terms of the two power terms in Eq. (5) to give us the following expression:

$$\Sigma = \left(\frac{1}{T_G} - \frac{1}{T_R} \right) \left(\left\langle \frac{k_B T_R}{RC(x)} \right\rangle - \left\langle \frac{V_R^2}{R} \right\rangle \right). \quad (7)$$

The entropy production for both temperature sweeps is shown in Fig. 6(a). The top line is the entropy produced when the resistor thermal bath temperature is increased, while the lower line is the entropy produced when the graphene thermal bath is increased. For equal temperatures, entropy production is zero for both cases because the systems are in thermodynamic equilibrium. For low temperatures, the entropy increases at the same rate for both cases. For high temperatures, the increase in entropy production with resistor temperature far outpaces the increase in entropy production with capacitor temperature.

The efficiency can be described as follows:

$$\epsilon = \frac{\left\langle \frac{d'W}{dt} \right\rangle}{\left\langle \frac{d'Q}{dt} \right\rangle}, \quad (8)$$

where the numerator is the power, which can be expressed as the absolute value of Eq. (5). The denominator is the heat flow

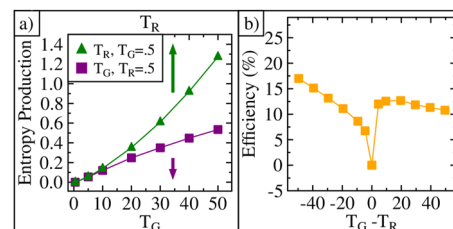


FIG. 6. Heat engine entropy and efficiency. (a) Entropy production as a function of thermal bath temperature. The top axis is the resistor and the bottom axis is the graphene. (b) Heat engine efficiency vs temperature differential between graphene and resistor.

from whichever reservoir is at the highest temperature. This can be expressed as follows:

$$\left\langle \frac{d'Q^*}{dt} \right\rangle = \begin{cases} \frac{\eta k_B T_G}{m}, & T_R < T_G, \\ \frac{k_B T_R}{RC}, & T_R > T_G. \end{cases} \quad (9)$$

The efficiency is then

$$\epsilon = \begin{cases} 1 - \frac{m \langle v^2 \rangle}{k_B T_G}, & T_R < T_G, \\ 1 - \frac{\langle V_R^2 \rangle}{\frac{k_B T_R}{C(x)}}, & T_R > T_G. \end{cases} \quad (10)$$

The efficiency of the heat engine is plotted as a function of the difference in the two thermal bath temperatures as shown in Fig. 6(b). When the resistor temperature is greater, the efficiency increases with the temperature difference in a linear manner. When the graphene temperature is larger, the efficiency at first increases but then plateaus. This is due to the graphene energy being higher than the double well.

VIII. SUMMARY

We modeled a system consisting of a graphene variable capacitor connected to a thermal bath, a resistor with its own thermal bath, and a battery. As the temperature of the graphene is raised and the resistor is kept fixed, we found that heat flows to the load resistor, and it dissipates extra power.

As the temperature of the resistor is raised and the graphene is kept fixed, we found that extra power is delivered to the graphene, and it produces more friction heat.

Entropy is produced in both cases. When the graphene is hotter, the entropy increases linearly. When the resistor is hotter, the entropy increases quadratically and is larger overall. The efficiency increases with increasing temperature but plateaus for the graphene.

In the simulations where the graphene temperature was increased, the variance of charge did increase. Thus, in a variable-RC circuit where the two elements are at different temperatures, the variance in the charge is modified due to the temperature of the capacitor, which is different from Nyquist's fixed-capacitor prediction.

As the charge variance increases, this can dramatically influence the movement of the graphene. This is because the electrostatic force pulling the graphene toward the electrode depends on the amount of instantaneous charge on the capacitor but does not depend on the sign of the charge.

It would be interesting to alter our friction to be frequency dependent, which may give rise to interesting dynamics.⁴⁵ These simulations show promise for increasing the power output of similar systems, such as graphene energy harvesting devices, by exploiting waste heat.

ACKNOWLEDGMENTS

This work was supported by the Walton Family Charitable Support Foundation (Grant No. RG3178).

AUTHOR DECLARATIONS

Conflict of Interest

The authors have no conflicts to disclose.

Author Contributions

J. Durbin: Data curation (equal); Formal analysis (equal); Investigation (equal); Methodology (equal); Software (equal); Validation (equal); Visualization (equal); Writing – original draft (equal); Writing – review & editing (equal). **J. M. Mangum:** Formal analysis (equal); Supervision (equal); Visualization (equal); Writing – original draft (equal); Writing – review & editing (equal). **M. N. Gikunda:** Data curation (equal); Formal analysis (equal); Validation (equal). **F. Harerimana:** Writing – original draft (equal); Writing – review & editing (equal). **T. Amin:** Writing – review & editing (equal). **P. Kumar:** Conceptualization (equal); Formal analysis (equal); Methodology (equal); Supervision (equal); Validation (equal). **L. L. Bonilla:** Formal analysis (equal); Methodology (equal); Supervision (equal); Validation (equal); Writing – review & editing (equal). **P. M. Thibado:** Conceptualization (equal); Formal analysis (equal); Funding acquisition (equal); Methodology (equal); Project administration (equal); Resources (equal); Software (equal); Supervision (equal); Validation (equal); Visualization (equal); Writing – original draft (equal); Writing – review & editing (equal).

DATA AVAILABILITY

The data that support the findings of this study are available from the corresponding author upon reasonable request.

REFERENCES

- S. Hanson, M. Seok, Y.-S. Lin, Z. Foo, D. Kim, Y. Lee, N. Liu, D. Sylvester, and D. Blaauw, "A low-voltage processor for sensing applications with picowatt standby mode," *IEEE J. Solid-State Circuits* **44**, 1145–1155 (2009).
- Y. Nonoguchi, K. Ohashi, R. Kanazawa, K. Ashiba, K. Hata, T. Nakagawa, C. Adachi, T. Tanase, and T. Kawai, "Systematic conversion of single walled carbon nanotubes into n-type thermoelectric materials by molecular dopants," *Sci. Rep.* **3**, 3344 (2013).
- C. Cho, K. L. Wallace, P. Tzeng, J.-H. Hsu, C. Yu, and J. C. Grunlan, "Outstanding low temperature thermoelectric power factor from completely organic thin films enabled by multidimensional conjugated nanomaterials," *Adv. Energy Mater.* **6**, 1502168 (2016).
- C. Wan and C. R. Bowen, "Multiscale-structuring of polyvinylidene fluoride for energy harvesting: The impact of molecular-, micro- and macro-structure," *J. Mater. Chem. A* **5**, 3091–3128 (2017).
- H. Im, H. G. Moon, J. S. Lee, I. Y. Chung, T. J. Kang, and Y. H. Kim, "Flexible thermocells for utilization of body heat," *Nano Res.* **7**, 443–452 (2014).
- M. Acerce, D. Voiry, and M. Chhowalla, "Metallic 1T phase MoS₂ nanosheets as supercapacitor electrode materials," *Nat. Nanotechnol.* **10**, 313–318 (2015).
- H. Huang, Y. Cui, Q. Li, C. Dun, W. Zhou, W. Huang, L. Chen, C. A. Hewitt, and D. L. Carroll, "Metallic 1T phase MoS₂ nanosheets for high-performance thermoelectric energy harvesting," *Nano Energy* **26**, 172–179 (2016).
- H. Sadeghi, S. Sangtarash, and C. J. Lambert, "Enhanced thermoelectric efficiency of porous silicene nanoribbons," *Sci. Rep.* **5**, 9514 (2015).
- A. Arnaud, J. Boughaleb, S. Monfray, F. Boeuf, O. Cugat, and T. Skotnicki, "Thermo-mechanical efficiency of the bimetallic strip heat engine at the macro-scale and micro-scale," *J. Micromech. Microeng.* **25**, 104003 (2015).

- ¹⁰O. Movilla Miangolarra, A. Taghvaei, R. Fu, Y. Chen, and T. T. Georgiou, "Energy harvesting from anisotropic fluctuations," *Phys. Rev. E* **104**, 044101 (2021).
- ¹¹V. Blicke and C. Bechinger, "Realization of a micrometre-sized stochastic heat engine," *Nat. Phys.* **8**, 143–146 (2012).
- ¹²R. Filliger and P. Reimann, "Brownian gyrator: A minimal heat engine on the nanoscale," *Phys. Rev. Lett.* **99**, 230602 (2007).
- ¹³J. Rosnagel, O. Abah, F. Schmidt-Kaler, K. Singer, and E. Lutz, "Nanoscale heat engine beyond the Carnot limit," *Phys. Rev. Lett.* **112**, 030602 (2014).
- ¹⁴M. Lopez-Suarez, R. Rurali, L. Gammaitoni, and G. Abadal, "Nanostructured graphene for energy harvesting," *Phys. Rev. B* **84**, 161401(R) (2011).
- ¹⁵N. Yang, G. Zhang, and B. W. Li, "Thermal rectification in asymmetric graphene ribbons," *Appl. Phys. Lett.* **95**, 033107 (2009).
- ¹⁶T. Ouyang, Y. Chen, Y. Xie, X. L. Wei, K. Yang, P. Yang, and J. Zhong, "Ballistic thermal rectification in asymmetric three-terminal graphene nanojunctions," *Phys. Rev. B* **82**, 245403 (2010).
- ¹⁷G. Zhang and H. Zhang, "Thermal conduction and rectification in few-layer graphene Y junctions," *Nanoscale* **3**, 4604–4607 (2011).
- ¹⁸X. Tong, X. Wang, S. Liu, H. Gao, R. Hao, and Y. Chen, "Low-grade waste heat recovery via an osmotic heat engine by using a freestanding graphene oxide membrane," *Acs Omega* **3**, 15501–15509 (2018).
- ¹⁹A. Bagri, S.-P. Kim, R. S. Ruoff, and V. B. Shenoy, "Thermal transport across twin grain boundaries in polycrystalline graphene from nonequilibrium molecular dynamics simulations," *Nano Lett.* **11**, 3917–3921 (2011).
- ²⁰Z. Gao, Y. Zhang, Y. Fu, M. M. F. Yuen, and J. Liu, "Thermal chemical vapor deposition grown graphene heat spreader for thermal management of hot spots," *Carbon* **61**, 342–348 (2013).
- ²¹R. Messina and P. Ben-Abdallah, "Graphene-based photovoltaic cells for near-field thermal energy conversion," *Sci. Rep.* **3**, 1383 (2013).
- ²²S. Philp, "Vacuum-insulated, varying-capacitance machine," *IEEE Trans. Electr. Insul.* **12**, 130–136 (1977).
- ²³F. Harerimana, H. Peng, M. Otobo, F. Luo, M. N. Gikunda, J. M. Mangum, V. P. Labella, and P. M. Thibado, "Efficient circuit design for low power energy harvesting," *AIP Adv.* **10**, 105006 (2020).
- ²⁴L. Wang and F. G. Yuan, "Vibration energy harvesting by magnetostrictive material," *Smart Mater. Struct.* **17**, 45009 (2008).
- ²⁵S. Roundy, P. K. Wright, and J. Rabaey, "A study of low level vibrations as a power source for wireless sensor nodes," *Comput. Commun.* **26**, 1131–1144 (2003).
- ²⁶M. Safaei, H. A. Sodano, and S. R. Anton, "A review of energy harvesting using piezoelectric materials: State-of-the-art a decade later (2008–2018)," *Smart Mater. Struct.* **28**, 113001 (2019).
- ²⁷J. S. Bunch, A. M. van der Zande, S. S. Verbridge, I. W. Frank, D. M. Tanenbaum, J. M. Parpia, H. G. Craighead, and P. L. McEuen, "Electromechanical resonators from graphene sheets," *Science* **315**, 490–493 (2007).
- ²⁸M. N. Gikunda, F. Harerimana, J. M. Mangum, S. Rahman, J. P. Thompson, C. T. Harris, H. O. H. Churchill, and P. M. Thibado, "Array of graphene variable capacitors on 100 mm silicon wafers for vibration-based applications," *Membranes* **12**, 533 (2022).
- ²⁹J. M. Mangum, F. Harerimana, M. N. Gikunda, and P. M. Thibado, "Mechanisms of spontaneous curvature inversion in compressed graphene ripples for energy harvesting applications via molecular dynamics simulations," *Membranes* **11**, 516 (2021).
- ³⁰M. L. Ackerman, P. Kumar, M. Neek-Amal, P. M. Thibado, F. M. Peeters, and S. Singh, "Anomalous dynamical behavior of freestanding graphene membranes," *Phys. Rev. Lett.* **117**, 126801 (2016).
- ³¹P. M. Thibado, P. Kumar, S. Singh, M. Ruiz-Garcia, A. Lasanta, and L. L. Bonilla, "Fluctuation-induced current from freestanding graphene," *Phys. Rev. E* **102**, 042101 (2020).
- ³²S. Panigrahi, A. Bhattacharya, S. Banerjee, and D. Bhattacharyya, "Interaction of nucleobases with wrinkled graphene surface: Dispersion corrected DFT and AFM studies," *J. Phys. Chem. C* **116**, 4374–4379 (2012).
- ³³W. L. Wang, S. Bhandari, W. Yi, D. C. Bell, R. Westervelt, and E. Kaxiras, "Direct imaging of atomic-scale ripples in few-layer graphene," *Nano Lett.* **12**, 2278–2282 (2012).
- ³⁴P. Xu, M. Neek-Amal, S. D. Barber, J. K. Schoelz, M. L. Ackerman, P. M. Thibado, A. Sadeghi, and F. M. Peeters, "Unusual ultra-low-frequency fluctuations in freestanding graphene," *Nat. Commun.* **5**, 3720 (2014).
- ³⁵H. Qin, Y. Sun, J. Z. Liu, M. Li, and Y. Liu, "Negative Poisson's ratio in rippled graphene," *Nanoscale* **9**, 4135–4142 (2017).
- ³⁶A. Fasolino, J. H. Los, and M. I. Katsnelson, "Intrinsic ripples in graphene," *Nat. Mater.* **6**, 858–861 (2007).
- ³⁷J. K. Schoelz, P. Xu, V. Meunier, P. Kumar, M. Neek-Amal, P. M. Thibado, and F. M. Peeters, "Graphene ripples as a realization of a two-dimensional Ising model: A scanning tunneling microscope study," *Phys. Rev. B* **91**, 045413 (2015).
- ³⁸C. Van den Broeck and M. Esposito, "Ensemble and trajectory thermodynamics: A brief introduction," *Physica A* **418**, 6–16 (2015).
- ³⁹U. Seifert, "Stochastic thermodynamics, fluctuation theorems and molecular machines," *Rep. Prog. Phys.* **75**, 126001 (2012).
- ⁴⁰U. Seifert, "Stochastic thermodynamics: Principles and perspectives," *Eur. Phys. J. B* **64**, 423–431 (2008).
- ⁴¹G. Benenti, G. Casati, K. Saito, and R. S. Whitney, "Fundamental aspects of steady-state conversion of heat to work at the nanoscale," *Phys. Rep.* **694**, 1–124 (2017).
- ⁴²I. A. Martínez, É. Roldán, L. Dinis, D. Petrov, J. M. R. Parrondo, and R. A. Rica, "Brownian Carnot engine," *Nat. Phys.* **12**, 67–70 (2016).
- ⁴³B. Gaveau, M. Moreau, and L. S. Schulman, "Stochastic thermodynamics and sustainable efficiency in work production," *Phys. Rev. Lett.* **105**, 060601 (2010).
- ⁴⁴H. Nyquist, "Thermal agitation of electric charge in conductors," *Phys. Rev.* **32**, 110–113 (1928).
- ⁴⁵R. Zwanzig, *Nonequilibrium Statistical Mechanics*, 1st ed. (Oxford University Press, 2001).